processes

MDPI

Article

Multi-Response Optimization during the High-Speed Drilling of Composite Laminate Using the Grey Entropy Fuzzy Method (GEF)

Jalumedi Babu [1,*], Anjaiah Madarapu [2], Lijo Paul [3], A. N. Khaleel Ahmed [1] and J. Paulo Davim [4]

[1] Department of Mechanical Engineering, IMPACT College of Engineering & Applied Sciences, Sahakaranagar South, Kodigenhalli, Bangalore 560092, Karnataka, India
[2] Department of Mechanical Engineering, Guru Nanak Institutions Technical Campus, Ibrahimpatnam, Hyderabad 501506, Telangana, India
[3] Department of Mechanical Engineering, St. Joseph's College of Engineering & Technology, Choondacherry, Kottayam 686579, Kerala, India
[4] Department of Mechanical Engineering, University of Aveiro Campus Santiago, 3810-183 Aveiro, Portugal
* Correspondence: dr.jalumedi.fac@iceas.ac.in or jalumedi.babu@gmail.com

Abstract: The machining of glass-fiber-reinforced composites is complex due to their heterogeneous structures. Research has indicated that high-speed machining, at high spindle speeds and feed rates, not only increases productivity but also reduces drilling defects, such as delamination. However, there are several challenges with high-speed machining, such as the heat generated during drilling between the drill tool and chip contact surfaces that can result in hole size errors. Therefore, it is essential to determine the optimum drilling parameters. This paper presents an innovative hybrid optimization approach called Grey Entropy Fuzzy. This approach is a combination of entropy-based weight integrated Grey Relation analysis and fuzzy logic. With the consideration of all responses simultaneously, an optimum machining combination was obtained at a spindle speed of 12,000 rpm and a feed rate of 0.02 mm/rev using a drill bit with a point angle of 118° and a drill diameter of 6 mm.

Keywords: composite materials; high-speed drilling; temperature; thrust force; delamination; Grey Entropy Fuzzy

Citation: Babu, J.; Madarapu, A.; Paul, L.; Ahmed, A.N.K.; Davim, J.P. Multi-Response Optimization during the High-Speed Drilling of Composite Laminate Using the Grey Entropy Fuzzy Method (GEF). *Processes* **2022**, *10*, 1865. https://doi.org/10.3390/pr10091865

Academic Editor: Zhou Li

Received: 4 August 2022
Accepted: 13 September 2022
Published: 15 September 2022

Table of Contents

1. Introduction

The perpetual challenge for the automotive and aerospace industry is to produce parts and assemblies that are lighter and more efficient. Defect-free drilling is very vital, as

drilling is the last machining activity, and reaming is generally not performed. Delamination at both the entry and exit of the hole is a critical drilling defect. Besides delamination, other drilling defects are variations in drill diameters, cylindricity and circularity errors. Ongoing research on composite materials explores ways of utilizing the advantages of high-speed machining. However, the quantity of research with high-speed drilling is much less as compared to the research on conventional low-speed drilling. The subsequent paragraphs present a brief review of research on the drilling of composite materials with conventional low-speed drilling and high-speed drilling.

Composite materials are designers' first option over traditional engineering materials utilized in the automotive, defense and aerospace manufacturing industries due to the growing demand for lightweight, rigid and strong materials [1]. Drilling is just one of the machining techniques used for structural joining. However, drilling operations, particularly high-speed drilling, are challenging with these materials due to their high heterogeneity and limited heat conductivity. Commonly observed defects include delamination, fiber pullout, matrix cracking and debonding [2–5]. The majority of investigations that are described in the literature concentrate on thrust force and its impact on drilling flaws, particularly delamination. Complete details about delamination and its techniques of measurement and evaluation are provided elsewhere [6–8].

Khashaba et al. [9,10] studied the impact of machining parameters during the drilling of GFRPCs both analytically and empirically, concentrating on thrust force and delamination. The impact of manufacturing processes on the mechanical characteristics of GFRP composites was investigated by Formisano et al. [11]. Erturk et al. [12] investigated how drilling parameters such as feed rate, spindle speed and drill bit geometry affect the delamination and temperature of GFRP composites. The employment of unconventional techniques to lessen delamination while machining GFRP composites is also a topic of the literature [13]. These tests were all carried out using standard low-speed drilling.

According to the authors, there have not been many investigations on the high-speed drilling of CFRP/GFRP composite laminates, which speeds up material removal. Delamination is also less common, and drilling costs are lower with high-speed drilling. The impact of high-speed drilling on delamination has been examined from various perspectives by several researchers. When Kao et al. [14] looked into coatings on micro-drills, they found that they enhanced the quality of the holes. In their investigation of the effects of thrust force and torque during drilling as well as hole quality, Lin et al. [15] concluded that, as spindle speed increased, the cutting force and, consequently, delamination decreased. According to research by Rubio et al. [16], high-speed drilling resulted in holes with higher quality. For high-speed composite drilling, Sanjay et al. [17] published machinability maps; the maps displayed the impact of the feed and spindle speed of rotation on circularity errors, delamination, surface roughness and hole size. They concluded that a machinability map can be utilized to determine the impact of changes in the operating forces on tool wear. The drilling settings were optimized by Vijayan Krishnaraj et al. [18], who found that feed had a significant effect on thrust and, consequently, on delamination damage. Other sources have also reported on the impact of spindle speeds and feeds during high-speed machining on delamination [19,20]. These previous studies on the high-speed machining of metal matrices [21] and CFRP composites [22] concentrate on delamination during drilling. Recently, in their review paper, Xia et al. [23] presented a variety of laser drilling methods, including short-pulsed laser drilling, long-pulsed laser drilling, ultrafast pulsed laser drilling and liquid-assisted laser drilling, for achieving high-quality and high-efficiency micro-hole drilling through controlling the laser–matter interaction. In another review, Xia et al. [24] presented a combined pulse laser (CPL) as a reliable tool for high-quality, high-efficiency material processing.

The primary aim of the present investigation was to explore the effect of spindle rotational speed, feed rate, drill bit point angle and diameter on thrust force, temperature, hole size and circularity errors as well as delamination at the exit and entry while drilling GFRPC laminates.

Recently, the Entropy-VIKOR approach was used by Perec and Musail [25] in the multi-criteria optimization of Abrasive Water Jet Cutting. Grey Relational Analysis was used in abrasive jet machining process optimization [26]. The combination of Entropy Grey Relational Analysis with fuzzy logic for such optimization is not available in the literature.

This study presents an innovative approach of combining entropy-based weight integrated Grey Relation Analysis with Fuzzy Logic, i.e., Grey Entropy Fuzzy (GEF), for the optimization of drilling variables during the high-speed drilling of composite materials.

2. Materials and Methods

Drilling experiments were conducted on a MAKINO S33 vertical machining center with 11 KW of power and a maximum spindle speed of 20,000 rpm, as shown in Figure 1. To conduct the drilling tests, the laminate was placed on the dynamometer, which was mounted on the bed of the machine. The drill bits used in the present study were uncoated carbide drills of diameters of 4, 6 and 8 mm with different point angles of 90°, 118° and 130° and a helix angle of 20°. The workpiece material used in the experiments was composed of woven fibers reinforced in an epoxy matrix. The composite was made in the size of 250 × 35 × 3 mm^3 with a density of 1.9 g/cm^3. For the experiment, four drilling conditions (feed rate, spindle speed, drill bit diameter and point angle) were used. Three levels were used for each control factor. Each experiment was conducted twice to obtain reliable results. The mean value of the tests was taken as the output response. The spindle speeds were 12,000, 15,000 and 18,000 rpm, the feeds were 0.02, 0.05 and 0.1 mm/rev, and drill bits with diameters of 4, 6 and 8 mm with different point angles of 90°, 118° and 130° were used. The machining conditions are shown in Table 1. The experiments were designed using an L-27 Orthogonal Array, as shown in Table 2.

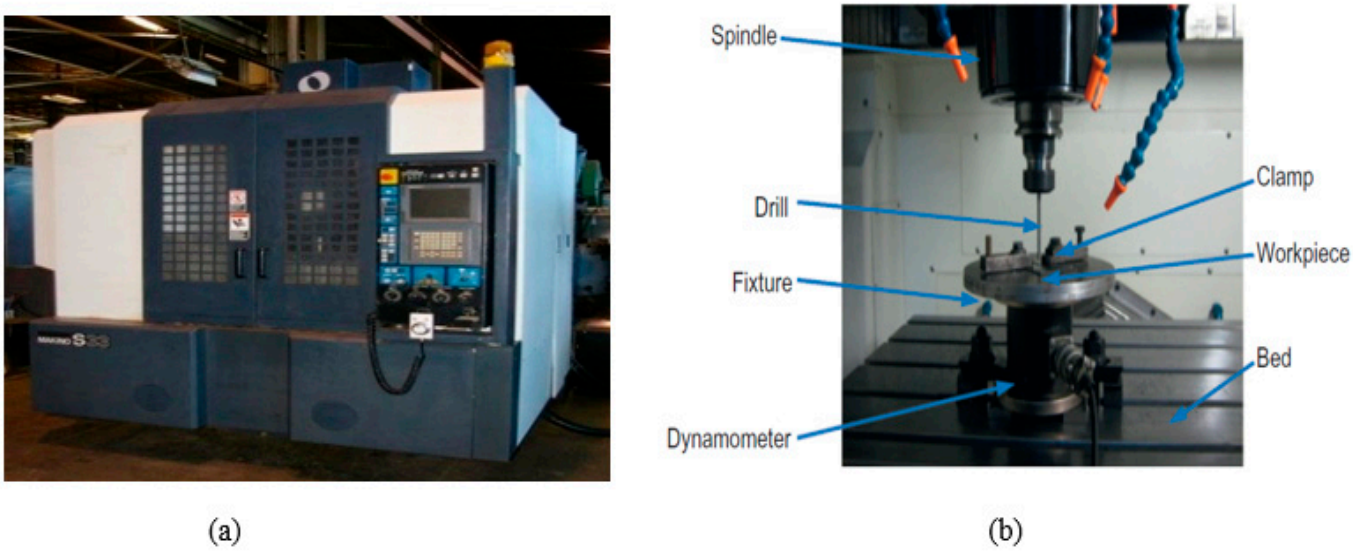

Figure 1. (**a**) Vertical machining center (**b**) Dynamometer arrangement for measuring thrust force [27].

Table 1. Machining conditions.

Drilling of the GFRP Laminate	
Equipment	Makino S33 VMC, with power 11 kW
Workpiece	GFRP 3 mm thick
Drilling Tools	Two-flute, 4, 6 and 8 mm diameter uncoated carbide (K20) drills of point angles 90°, 118° and 130°
Drilling Conditions	Spindle speed—12,000, 15,000 and 18,000 rpm, Feed (mm/rev) 0.02, 0.05 and 0.1

Table 2. Taguchi's l–27 orthogonal array.

Exp No.	Spindle Speed, rpm	Feed Rate, mm/rev	Point Angle, Degrees	Drill Diameter, mm
1	12,000	0.02	90	4
2	12,000	0.02	118	6
3	12,000	0.02	130	8
4	12,000	0.05	90	6
5	12,000	0.05	118	8
6	12,000	0.05	130	4
7	12,000	0.1	90	8
8	12,000	0.1	118	4
9	12,000	0.1	130	6
10	15,000	0.02	90	6
11	15,000	0.02	118	8
12	15,000	0.02	130	4
13	15,000	0.05	90	8
14	15,000	0.05	118	4
15	15,000	0.05	130	6
16	15,000	0.1	90	4
17	15,000	0.1	118	6
18	15,000	0.1	130	8
19	18,000	0.02	90	8
20	18,000	0.02	118	4
21	18,000	0.02	130	6
22	18,000	0.05	90	4
23	18,000	0.05	118	6
24	18,000	0.05	130	8
25	18,000	0.1	90	6
26	18,000	0.1	118	8
27	18,000	0.1	130	4

Using a (Syscon SI-223D) dynamometer, the thrust forces during milling were measured. The forces experienced during drilling were measured and stored using a digital storage oscilloscope. The complete details are presented elsewhere [27]. A flat-bed scanner with a resolution of 1200 PPI was used to scan the drilled sheet, and the amount of delamination was then recorded as a bitmap image. These pictures were then uploaded to the "Image J" program for additional editing. Then, binary pictures of color images were created. The histogram of the delaminated area and the undamaged area was compared to determine the threshold for the transition. The image processing method used to generate the delaminated region with acceptable quality is illustrated in Figure 2. The temperatures during the drilling tests were measured using an FLIR E-50 Thermal Imager. The camera used in this was an Uncooled Focal Plane Array (UFPA) detector. The temperature range of this thermal imager was −20 °C to 650 °C. The instrument was calibrated with known temperatures initially. The circularity error and hole size error were calculated using coordinate measuring equipment. MATLAB R2021a and Minitab 20 were used for the analysis of output responses and optimization.

The delamination factor was calculated as the ratio of the delaminated area (A_d) to the nominal area of the hole (A_o) with Equation (1).

$$F_d = \frac{A_d}{A_o} \quad (1)$$

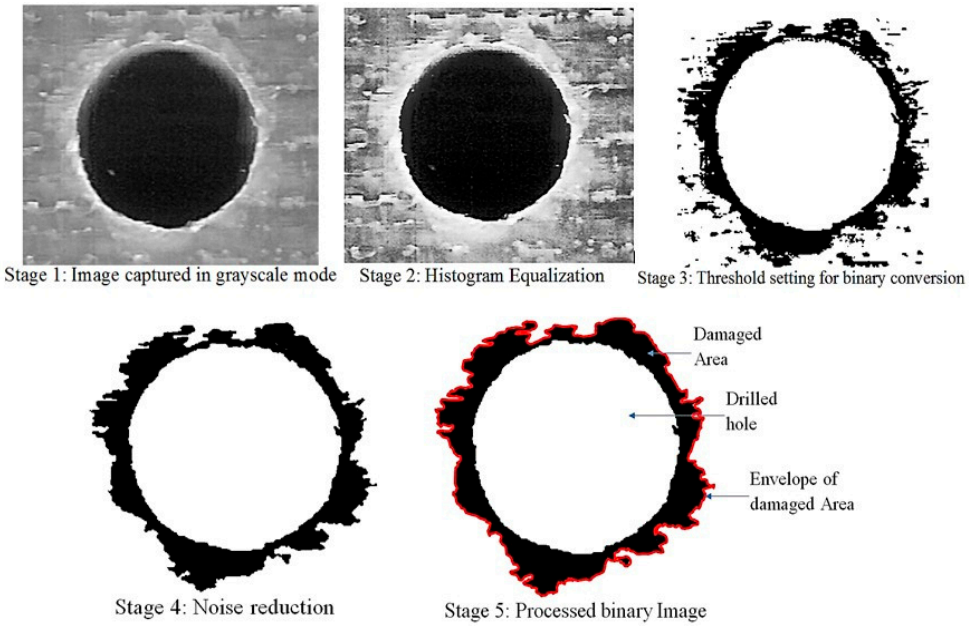

Figure 2. Image processing procedure [27].

3. Results and Discussion

Table 3 lists the output responses for various drilling situations, including both peel-up and push-out delamination, thrust force, temperature, hole size errors and circularity errors.

Table 3. Experimental results.

Experiment No.	Thrust Force (N)	Temperature, °C	Hole Size Error, mm	Circularity Error, mm	Delamination Factor	
					Peel-Up	Push-Out
1	15.10	86.00	0.0415	0.0060	1.1650	1.0700
2	20.00	86.50	0.1920	0.0210	1.0740	1.0520
3	52.50	90.00	0.0130	0.0170	1.0310	1.0303
4	42.00	106.0	0.0430	0.0255	1.0595	1.0420
5	48.50	89.50	0.0215	0.0085	1.0484	1.0307
6	69.00	88.50	0.0975	0.1920	1.0742	1.1500
7	189.0	76.75	0.0970	0.0295	1.0502	1.0405
8	93.75	93.00	0.0030	0.0220	1.1550	1.2060
9	77.50	88.50	0.0250	0.0175	1.0825	1.0735
10	41.50	104.5	0.2790	0.0175	1.0960	1.0530
11	22.00	86.00	0.1035	0.0465	1.0502	1.0440
12	25.00	76.75	0.1860	0.1345	1.1420	1.1090
13	133.0	129.0	0.2020	0.0300	1.0470	1.0250
14	38.00	85.00	0.0290	0.0055	1.1300	1.1205
15	109.5	72.50	0.9885	0.0130	1.0535	1.0760
16	31.00	115.0	0.0795	0.0590	1.1940	1.1700
17	48.50	104.5	0.0220	0.0070	1.1080	1.0850
18	65.00	103.5	0.0465	0.0130	1.0510	1.0420
19	117.5	142.5	0.1010	0.0120	1.0425	1.0415
20	17.50	76.50	0.1455	0.2795	1.1150	1.1505
21	78.00	90.00	0.9750	0.0090	1.0535	1.0575
22	21.50	99.50	0.0270	0.0075	1.2100	1.2020
23	35.50	115.0	0.3175	0.1500	1.0710	1.0550
24	63.00	96.00	0.0510	0.0070	1.0465	1.0535
25	46.50	103.5	0.2625	0.0165	1.0900	1.0825
26	22.50	94.00	0.1900	0.0160	1.0465	1.0390
27	41.50	80.50	0.0170	0.0065	1.1900	1.2600

From Table 3, the S/N ratios of the output responses were calculated, and the main effect plots of these responses were made and are presented in Figures 3–5 to know the influence of the input factors on the output responses and the optimum conditions for each output response.

The thrust force was observed to decrease with an increase in spindle speed, as implied by Figure 3a. This is due to a rise in temperature, which causes the matrix to soften. Due to a rise in uncut chip size and more fiber impact, the thrust force increases with feed [18]. Additionally, it was shown that a greater drill diameter and tip angle both boosted thrust forces. This is explained by the fact that a larger drill diameter produces a hole with a larger contact area, increasing the thrust force [16]. The S/N graph in Figure 3a shows that a feed rate of 0.02 mm/rev, a spindle speed of 18,000 rpm, a drill diameter of 4 mm and a point angle of 118° are the optimum values for the thrust force.

It is clear from Figure 3b that temperature rises as the feed rate and spindle speed increase. In both situations, raising the cutting conditions results in a higher energy conversion and, as a result, a higher loss of mechanical energy as heat and greater friction between the workpiece and the cutting edge, generating the heat. In contrast, increased feed rates caused the cutting edge's contact length to be reduced. According to this theory, the clearing face and minor cutting edges should experience less friction, which should result in a minimal amount of heat buildup [28].

(a)

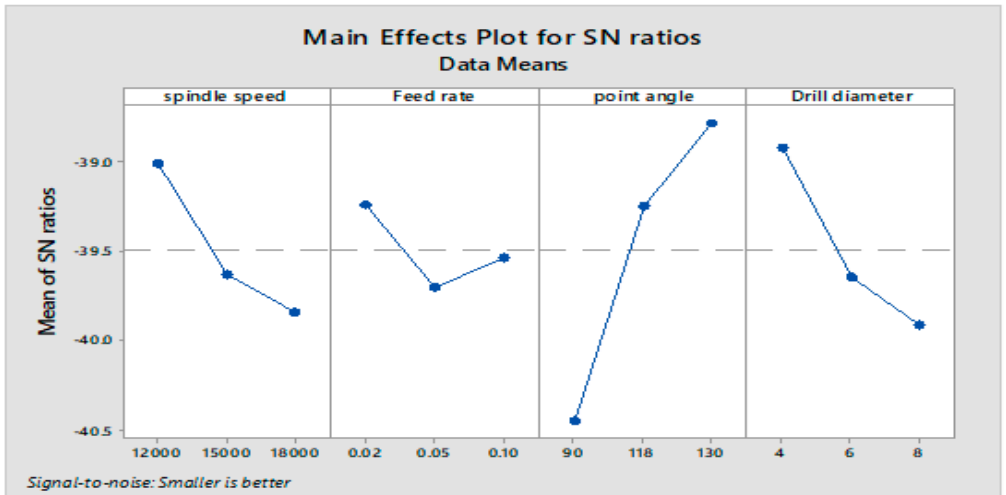

(b)

Figure 3. Main-effects plots for S/N ratios of (**a**) Thrust force and (**b**) Temperature.

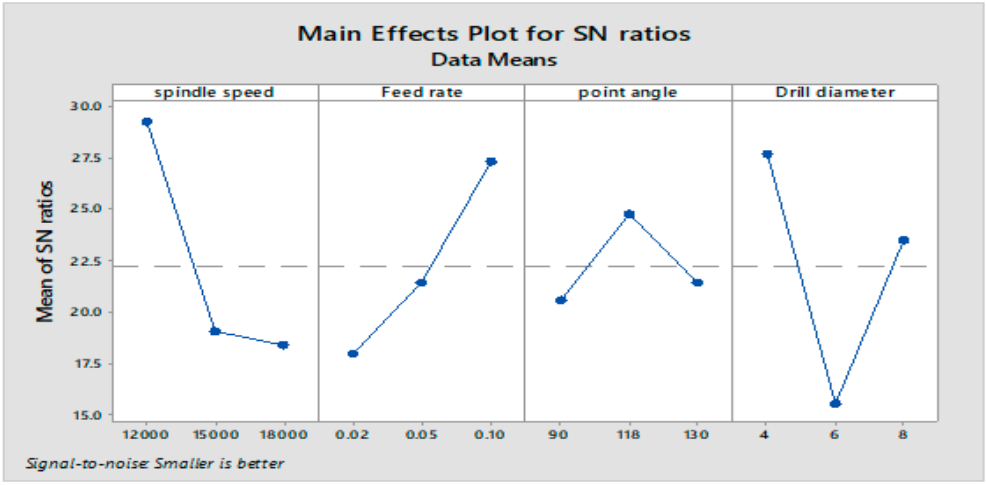

(a)

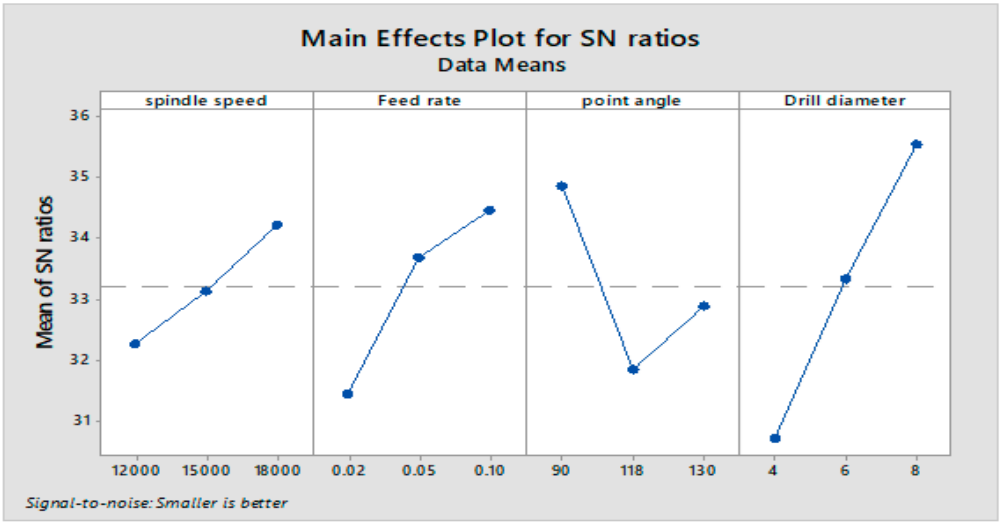

(b)

Figure 4. Main effects plots for S/N ratios of (**a**) Hole size errors and (**b**) Circularity errors.

With an increase in point angle, temperature was observed to drop. The figure clearly shows that the tool's temperature rose as drill diameter increased. The size of the contact area between the workpiece and the drill bit determines how much friction is generated during drilling [29]. The contact surface increases with a larger drillbit diameter, causing higher friction. The tool's temperature rises as a result of more intense heat generation during drilling.

The combination of spindle speed level 3 (20,000 rpm), feed rate level 1 (0.02 mm/rev), point angle level 1 (90°) and drill diameter level 3 (6 mm) produced the highest temperature of 142 °C. This is closer to the temperature at which glass transitions occur, which could weaken the material and cause degradation. The huge contact area and high spindle speeds that produce faster cutting speeds may be the cause of the higher temperature (due to the larger drill diameter). Due to the limited thermal conductivity of the material and slow heat dissipation to the rest of the work piece, the low feed rate emphasizes the temperature rise.

The temperature at the tool–workpiece interface continues to rise as a result of tool wear brought on by heat at the cutting zone. The highest temperature is anticipated at the hole's exit among the three drilling stages of the entrance, drilling while inside the work piece, and the exit. Additionally, mechanical delamination occurs in this region [30]. At the hole's opening, both factors combine to cause combined heat and mechanical

damage. At higher temperatures, thermal degradation can cause fissures that can start delamination and weaken a material [31,32]. Under the glass transition temperature, the cutting temperature ought to be managed. A decrease in the composite's strength and the occurrence of severe flaws such as delamination are anticipated when the temperature exceeds the glass transition temperature.

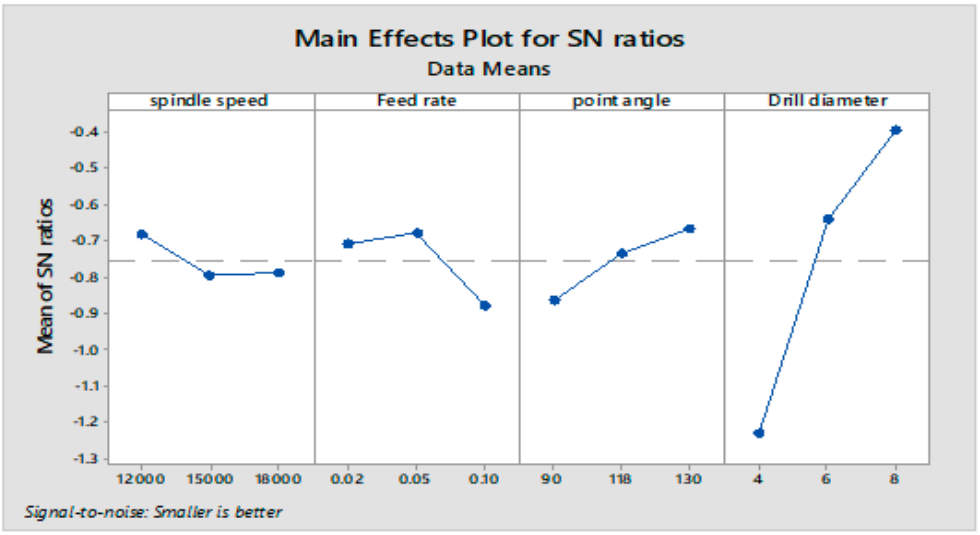

(a)

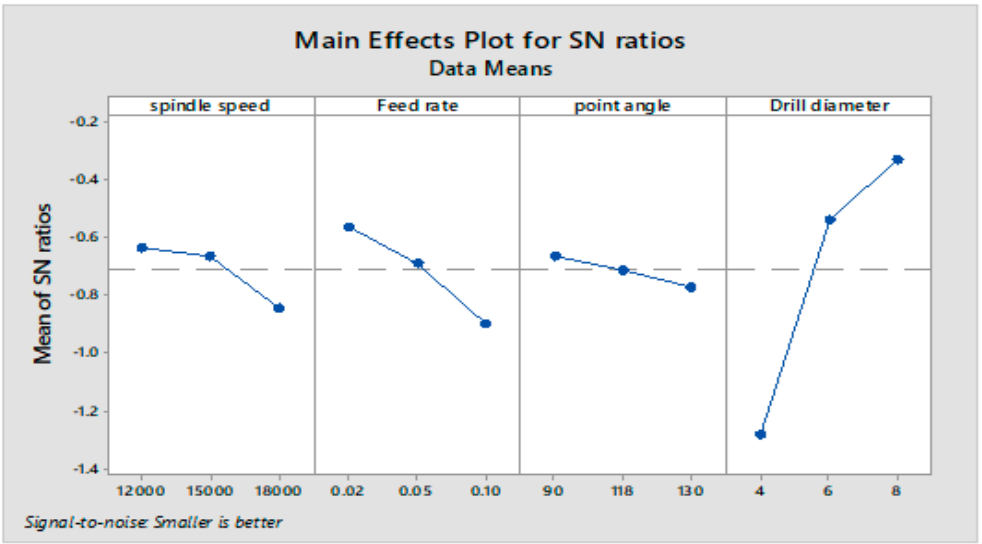

(b)

Figure 5. Main effects plots for S/N ratios of (**a**) Peel-up delamination and (**b**) Pushout delamination.

The S/N graph in Figure 3b shows that a spindle speed of 12,000 rpm, a point angle of 130°, a feed rate of 0.02 mm/rev and a drill diameter of 4 mm are the optimum combination of input parameters for temperature.

According to Figure 4a, frictional heating causes the cutting temperature to increase at high spindle speeds and a low feed, increasing the hole size inaccuracy. Smaller uncut chip thicknesses at lower feeds lead to larger shear forces, which in turn increase vibration, increasing the specific cutting resistance. At lower feeds, the hole size inaccuracy increases; at higher feeds, it decreases. The ploughing movement that causes the heating effect caused by friction severely damages the matrix and pulls out the fibers. The size effect results from this can be seen in [18].

The hole size error may also be a result of the matrix degrading and fibers being pulled out by the ploughing motion that causes temperature to rise, owing to friction [18]. The impact of matrix softening during high-speed drilling regarding mechanical and thermal damages, according to Khashaba [33], is not entirely known. The contact surface grows as the drill bit diameter rises, which increases friction. Cutting speed increases with increasing drill diameter, which leads to heat degradation and, ultimately, hole size inaccuracy. In the literature, similar increases in hole diameters (hole size errors) are documented [17–20].

The S/N plot indicates a spindle speed of 12,000 rpm, a feed rate of 0.10 mm/rev, a point angle of 118° and a drill diameter of 4 mm are the optimum combination of input parameters for the hole size error.

According to Figure 4b, it can be seen that the circularity decreases with an increase in spindle speed and feed. The rotational stability of the drill is better at higher speeds than it is at lower speeds. This explains the lesser circularity error at high speeds. A low feed rate of 0.02 mm/rev creates greater circularity error. This may be because of ploughing and frictional heating [18]. The S/N chart shows that a spindle speed of 18,000 rpm, a feed rate of 0.10 mm/rev, a point angle of 90° and a drill diameter of 8 mm are the ideal combination of input parameters for achieving the lowest possible circularity error.

It is clear from Figure 5a that spindle speeds that produce less delamination than those that produce more delamination are substantially lower. According to Gaitonde et al. [27], this behavior is attributed to the fact that increasing speed raises the temperature, which encourages matrix softening and, in turn, increases delamination. This is consistent with the trend noted by Krishnaraj et al. [18]. Typically, at high feed rates, the built-up edge is created on the tool as a result of increased heat generation, which causes significant tool wear and, consequently, an increase in delamination [30]. According to the S/N chart in Figure 5a, the ideal combination of input parameters for minimum peel-up delamination is a spindle speed of 12,000 rpm, a point angle of 130°, a feed rate of 0.05 mm/rev and a drill diameter of 8 mm.

The push-out delamination factor rises with an increase in feed rate and spindle speed, as shown in Figure 5b. The thrust force increases together with the feed rate. In the studies, the spindle speed and feed rate increases were accompanied by an increase in the delamination ratio. This may be a result of the GFRP laminates' thinner thickness. Due to the matrix heating at high spindle speeds, which results in decreased stiffness, delamination may begin at lower cutting forces [18]. The built-up edge is typically generated on tools at high feed rates because of increased heat generation, which leads to significant tool wear and, consequently, an increase in delamination. Figure 5b also shows that the delamination factor is minimal at smaller point angles. The reduction in thrust force at low point angles, which in turn lowers delamination damage, may be the cause [30]. According to the S/N graph in Figure 5b, the ideal combination of input parameters for push-out delamination is a spindle speed of 12,000 rpm, a point angle of 90°, a feed rate of 0.02 mm/rev and a drill diameter of 8 mm.

Spindle speed and feed rate are the main cutting factors that affect the mechanism of damage. High spindle speeds generate heat, and the amount of time it takes for this heat to build up at the surface and burn the matrix affects delamination damage. The feed rate affects how long it takes to cut. The delamination of composite materials may be significantly influenced by temperature increases during drilling. A rise in temperature that is moderate may help to prevent delamination, and an increase that is more extreme and that approaches or exceeds the glass transition temperature weakens the composite material and may enhance delamination [32].

The temperature of the cutting zone and the tool generally rises as spindle speed and cutting speed increase; this increase in temperature may have either a favorable or unfavorable impact on the delamination damage (work piece). According to Gaitonde et al. [34,35], the primary driving force behind the delamination is a cutting force occurring in the peripheral direction. This increase in temperature has the potential to change the tool's size and shape as well as the effectiveness of the coating material, both of which have an impact

on how well the drilling operation works as a whole. The impact of matrix softening on delamination regarding thermal and mechanical damages has not yet been extensively examined, according to Khashaba [33], and issues still need to be resolved.

The optimum conditions of input factors for individual output responses are shown in Table 4.

Table 4. Optimum machining conditions for individual responses.

Sl. No.	Process Parameter	Taguchi Optimization Method for Individual Responses, Optimum Values					
		Thrust Force	Temperature	Hole Size Error	Circularity Error	Peel-Up Delamination	Push-Out Delamination
1	Spindle speed, rpm	18,000	12,000	12,000	18,000	12,000	12,000
2	Feed rate, mm/rev	0.02	0.02	0.10	0.10	0.05	0.02
3	Point angle, degree	118	130	118	90	130	90
4	Drill diameter, mm	4	4	4	8	8	8

In order to obtain optimum drilling conditions for all these multi-responses simultaneously, an innovative approach, Grey Entropy Fuzzy is used for the optimization of drilling variables during the high-speed machining of composite materials.

4. Optimization with Entropy-Weight-Based Grey Relational Analysis

4.1. Grey Relational Analysis

Grey Relational analysis (GRA) is used to optimize high-speed drilling during the machining of GFRP composite laminate sheets. One quantitative method for determining inequality and equality between input conditions is the generalized additive model. It is necessary to equalize the values of the replies in the range between 1 and 0 because each output response has a different range and unit. This may be required to view some responses in multi-objective optimization problems as maximization (higher is better), other responses as minimization (smaller is better) and some responses as a nominal value, which is the better type. Multi-response issues are reduced by GRA to a single response called the Grey Relational Coefficient.

Responses for maximization are normalized with Equation (2).

$$X_i^*(k) = \frac{X_i^0(k) - min X_i^0(k)}{max X_i^0(k) - \min X_i^0(k)} \quad (2)$$

Responses for minimization are normalized with Equation (3).

$$X_i^*(k) = \frac{max\ X_i^0(k) - X_i^0(k)}{max X_i^0(k) - \min X_i^0(k)} \quad (3)$$

Responses for the nominal values, the better type, are normalized with Equation (4).

$$X_i^* = 1 - \frac{\left|X_i^0(k) - X^0\right|}{\max\ X_i^0(k) - X_i^0} \quad (4)$$

$i = 1, 2, 3 \ldots, n$;
n is the number of drilling parameters;
m is the amount of experiment data;
$X_i^0(k)$ is the original sequence;
$X_i^*(k)$ is the sequence after data pre-processing;
max $X_i^0(k)$ is the largest value in $X_i^0(k)$;
min $X_i^0(k)$ = the smallest value in $X_i^0(k)$;
X^0 = the desired value.
Normalized values that are calculated for the responses are shown in Table 5.

Table 5. Normalized values and deviation sequences of the output responses.

Experiment No.	Normalized Values						Deviation Sequence					
	A	B	C	D	E	F	A	B	C	D	E	F
1	1.0000	0.8071	0.9609	1.0000	0.2514	0.8085	0.0000	0.1929	0.0391	0.0000	0.7486	0.1915
2	0.9718	0.8000	0.8082	0.9452	0.7598	0.8851	0.0282	0.2000	0.1918	0.0548	0.2402	0.1149
3	0.7849	0.7500	0.9899	0.9598	1.0000	0.9774	0.2151	0.2500	0.0101	0.0402	0.0000	0.0226
4	0.8453	0.5214	0.9594	0.9287	0.8408	0.9277	0.1547	0.4786	0.0406	0.0713	0.1592	0.0723
5	0.8079	0.7571	0.9812	0.9909	0.9028	0.9757	0.1921	0.2429	0.0188	0.0091	0.0972	0.0243
6	0.6901	0.7714	0.9041	0.3199	0.7587	0.4681	0.3099	0.2286	0.0959	0.6801	0.2413	0.5319
7	0.0000	0.9393	0.9046	0.9141	0.8927	0.9340	1.0000	0.0607	0.0954	0.0859	0.1073	0.0660
8	0.5477	0.7071	1.0000	0.9415	0.3073	0.2298	0.4523	0.2929	0.0000	0.0585	0.6927	0.7702
9	0.6412	0.7714	0.9777	0.9580	0.7123	0.7936	0.3588	0.2286	0.0223	0.0420	0.2877	0.2064
10	0.8482	0.5429	0.7199	0.9580	0.6369	0.8809	0.1518	0.4571	0.2801	0.0420	0.3631	0.1191
11	0.9603	0.8071	0.8980	0.8519	0.8927	0.9191	0.0397	0.1929	0.1020	0.1481	0.1073	0.0809
12	0.9431	0.9393	0.8143	0.5302	0.3799	0.6426	0.0569	0.0607	0.1857	0.4698	0.6201	0.3574
13	0.3220	0.1929	0.7981	0.9122	0.9106	1.0000	0.6780	0.8071	0.2019	0.0878	0.0894	0.0000
14	0.8683	0.8214	0.9736	1.0018	0.4469	0.5936	0.1317	0.1786	0.0264	0.0018	0.5531	0.4064
15	0.4572	1.0000	0.0000	0.9744	0.8743	0.7830	0.5428	0.0000	1.0000	0.0256	0.1257	0.2170
16	0.9086	0.3929	0.9224	0.8062	0.0894	0.3830	0.0914	0.6071	0.0776	0.1938	0.9106	0.6170
17	0.8079	0.5429	0.9807	0.9963	0.5698	0.7447	0.1921	0.4571	0.0193	0.0037	0.4302	0.2553
18	0.7131	0.5571	0.9559	0.9744	0.8883	0.9277	0.2869	0.4429	0.0441	0.0256	0.1117	0.0723
19	0.4112	0.0000	0.9006	0.9781	0.9358	0.9298	0.5888	1.0000	0.0994	0.0219	0.0642	0.0702
20	0.9862	0.9429	0.8554	0.0000	0.5307	0.4660	0.0138	0.0571	0.1446	1.0000	0.4693	0.5340
21	0.6383	0.7500	0.0137	0.9890	0.8743	0.8617	0.3617	0.2500	0.9863	0.0110	0.1257	0.1383
22	0.9632	0.6143	0.9756	0.9945	0.0000	0.2468	0.0368	0.3857	0.0244	0.0055	1.0000	0.7532
23	0.8827	0.3929	0.6809	0.4735	0.7765	0.8723	0.1173	0.6071	0.3191	0.5265	0.2235	0.1277
24	0.7246	0.6643	0.9513	0.9963	0.9134	0.8787	0.2754	0.3357	0.0487	0.0037	0.0866	0.1213
25	0.8194	0.5571	0.7367	0.9616	0.6704	0.7553	0.1806	0.4429	0.2633	0.0384	0.3296	0.2447
26	0.9574	0.6929	0.8102	0.9634	0.9134	0.9404	0.0426	0.3071	0.1898	0.0366	0.0866	0.0596
27	0.8482	0.8857	0.9858	0.9982	0.1117	0.0000	0.1518	0.1143	0.0142	0.0018	0.8883	1.0000

4.2. Grey Relational Coefficient

The Grey Relational Coefficient is calculated with Equation (5).

$$\xi(k) = \frac{\Delta_{min} + \zeta\Delta_{max}}{\Delta_{0i}(k) + \zeta\Delta_{max}} \tag{5}$$

$\Delta_{0i}(k)$, Δ_{max} and Δ_{min} are calculated using Equations (6)–(8).

$$\Delta_{0i}(k) = \|X_0^*(k) - X_i^*(k)\| \tag{6}$$

$$\Delta_{max} = \text{maxmax}\, \|X_0^*(k) - X_i^*(k)\| \tag{7}$$

$$\Delta_{min} = \text{minmin}\, \|X_0^*(k) - X_i^*(k)\| \tag{8}$$

ζ = the identification coefficient in the range of ζ [0, 1]. In general, ζ = 0.5.

where $\Delta_{0i}(k)$ = the deviation sequence for the reference sequence;

$X_0^*(k)X_i^*(k)$ is the comparability sequence.

The values Δ_{max} and Δ_{min} can be found in Table 4. The Grey Relational Coefficients obtained with Equation (5) for all drilling conditions are shown in Table 5. The deviation sequence obtained after data pre-processing is also shown in Table 5.

The following notations are used for the responses.

A—Thrust Force;

B—Temperature;

C—Hole size Error;

D—Circularity Error;

E—Peel-up Delamination Factor;

F—Push-out Delamination Factor.

4.3. Grey Relational Grade

The Grey Relational Grade is calculated as the average of all the Grey Relational Coefficients of individual responses, as given in Equation (9). This equation can be used only when all the responses are assigned an equal weight.

$$GRG = \frac{1}{n}\sum_{k=1}^{n}\zeta_i(\mathrm{k}) \quad (9)$$

$$GRG = \frac{1}{n}\sum_{k=1}^{n} W_k\,\zeta_i(k),\ \ \sum_{k=1}^{n} W_k = 1 \quad (10)$$

where W_k shows the normalized weight of response k. For equal weights, Equations (9) and (10) are the same.

In the current work, an objective method, i.e., the entropy method [36,37], is used in the calculation of the weightages for all the responses. The comprehensive procedure is given below.

4.4. Entropy Method

Weaver and Shanon created this technique in 1947, and Zeleney improved it in 1982 to determine the objective weights of each response. Entropy is essentially a measurement of the degree of uncertainty in the information or data. It makes use of probability theory. The data are normalized using Equations (2) and (3) to determine weights by the entropy approach, and Equations (2) and (3) are then used to find the associated entropy values for each response (11).

$$e_j = -\frac{1}{lnm}\sum_{i=1}^{m} P_{ij}\ln P_{ij} \quad (11)$$

Here $P_{ij} = \frac{y_{ij}}{\sum_{i=1}^{m} y_{ij}}$, and m is the total no. of tests conducted. In this study, m = 27. The performance response increases or decreases with the entropy (e_j). The individual weights can be calculated with Equation (12).

$$w_j = \frac{(1-e_j)}{\sum_{i=1}^{n}(1-e_j)} \quad (12)$$

The calculated normalized, P_{ij}, and $P_{ij}\ln P_{ij}$ values for the responses are shown in Supplementary Table S1. Now, using these values, the entropy and weights are calculated for the responses using Equations (11) and (12), respectively. The values obtained are shown in Table 6.

Table 6. Calculation of weightages of output responses.

Response	e_j	$(1-e_j)$	w_j
A	0.9799	0.0201	14
B	0.9767	0.0233	17
C	0.9760	0.0240	17
D	0.9818	0.0182	13
E	0.9683	0.0317	23
F	0.9773	0.0227	16
Sum		0.1400	100

The calculated weights, using Equation (12), that were obtained for the responses of thrust force, temperature, hole size error, circularity error, peel-up/entry delamination factor and push-out/exit delamination factors are 0.14, 0.17, 0.17, 0.13, 0.23 and 0.16, respectively. The same values are considered in the calculation of Grey Relational Grade using Equation (10). Table 7 represents the obtained Grey Relational Coefficients, Grey Relational Grade and the rank for all the test runs.

Table 7. Grey Relational Coefficients with entropy-based weights, Grey Relational Grade and rank for the various test runs.

Experiment No.	Grey Relational Coefficients						Grey Relational Entropy Grade	Rank
	A (0.14)	B (0.17)	C (0.17)	D (0.13)	E (0.23)	F (0.16)		
1	1.0000	0.7216	0.9275	1.0000	0.4004	0.7231	0.7794	8.5
2	0.9467	0.7143	0.7228	0.9012	0.6755	0.8131	0.8813	1
3	0.6992	0.6667	0.9801	0.9255	1.0000	0.9568	0.7790	10
4	0.7637	0.5109	0.9249	0.8752	0.7585	0.8736	0.8522	2
5	0.7225	0.6731	0.9638	0.9820	0.8372	0.9537	0.6335	25
6	0.6173	0.6863	0.8391	0.4237	0.6745	0.4845	0.7827	7
7	0.3333	0.8917	0.8398	0.8534	0.8234	0.8835	0.6265	26
8	0.5251	0.6306	1.0000	0.8953	0.4192	0.3936	0.7401	11
9	0.5822	0.6863	0.9573	0.9224	0.6348	0.7078	0.6875	18
10	0.7671	0.5224	0.6410	0.9224	0.5793	0.8076	0.8210	3
11	0.9265	0.7216	0.8306	0.7715	0.8234	0.8608	0.6642	21
12	0.8978	0.8917	0.7292	0.5156	0.4464	0.5831	0.7113	16
13	0.4245	0.3825	0.7123	0.8507	0.8483	1.0000	0.7255	13
14	0.7915	0.7368	0.9499	1.0037	0.4748	0.5516	0.7128	14
15	0.4795	1.0000	0.3333	0.9513	0.7991	0.6973	0.5891	27
16	0.8454	0.4516	0.8656	0.7207	0.3545	0.4476	0.7122	15
17	0.7225	0.5224	0.9629	0.9927	0.5375	0.6620	0.7868	6
18	0.6354	0.5303	0.9189	0.9513	0.8174	0.8736	0.7314	12
19	0.4592	0.3333	0.8341	0.9580	0.8861	0.8769	0.6600	22
20	0.9731	0.8974	0.7757	0.3333	0.5159	0.4835	0.6881	17
21	0.5802	0.6667	0.3364	0.9785	0.7991	0.7833	0.6576	23
22	0.9314	0.5645	0.9536	0.9892	0.3333	0.3990	0.6437	24
23	0.8100	0.4516	0.6104	0.4871	0.6911	0.7966	0.8008	5
24	0.6448	0.5983	0.9112	0.9927	0.8524	0.8048	0.6711	20
25	0.7347	0.5303	0.6550	0.9287	0.6027	0.6714	0.8177	4
26	0.9216	0.6195	0.7249	0.9319	0.8524	0.8935	0.6768	19
27	0.7671	0.8140	0.9724	0.9964	0.3602	0.3333	0.7794	8.5

4.5. Optimization with GREG

In Table 7, Experiment Number 2 shows the maximum value of the GREG, which represents the optimum combination of input parameters. The GREG values vary from 0.5891 to 0.8813. Therefore, from Table 3, the experimental values of all responses at optimized machining conditions are a thrust force of 20 N, a temperature of 86.5 °C, a hole size error of 0.1920, a circularity error of 0.0210, a peel-up delamination factor of 1.074 and a push-out delamination factor of 1.052.

5. Optimization Using the Grey Entropy Fuzzy Method (GEFM)

The above-mentioned methods, such as entropy and Grey Relational Analysis, have uncertainty and limitations due the use of higher-the-better, nominal-the-better, and lower-the-better performance characteristics in the optimization process, such as high-speed drilling. However, these methods are effective and efficient in converting multi-objective problems to single-objective problems [38–40].

Early optimization research studies either employed subjective methods such as the SIMO technique or applied the same weights to all answers, which are insufficient or incorrect ways to improve the process parameters. Therefore, to reduce a multi-objective problem to a single objective called GREG, the entropy approach, an objective method, is employed along with GRA to determine the majority of scientific objective weights. Complex multi-objective optimization problems can thus be resolved by combining the entropy technique, fuzzy logic and Grey Relational Analysis [41–43].

Grey Entropy Fuzzy Method

As previously described, GREG includes weighted sums based on entropy for each of the six Grey Relational Coefficients. As a result, the GREG problem can be optimized without taking response criteria into account. For this, the GEFG desirability function is applied using the fuzzy model while considering all input variables. The initial phases in a fuzzy model are the fuzzification of the output and input data, the development of fuzzy rules and the eventual defuzzification of the outputs or outcomes.

Later, the corresponding GEFG values are calculated using MATLAB's fuzzy logic toolbox (R2021a). The inputs to the fuzzy logic system are the GREG values of the thrust force, temperature, hole size error, circularity error, peel-up and push-out delamination factors and triangle membership functions, which are employed for the fuzzy modelling. Nine linguistic membership functions are used for the input and output of the Grey Entropy Fuzzy Grade: lowest (LT), very low (VL), medium low (ML), low (L), medium high (MH), high (H), medium higher (MHR), higher (HR) and highest (HT). In Figure 6, these membership functions are displayed.

Figure 7 displays the calculated GEFG values as they appear in the fuzzy rule viewer. Twenty-seven rows in this diagram depict the fuzzy rules that were applied, and six columns in it represent the GRC values of the thrust force, temperature, hole size error, circularity error and peel-up and push-out delamination factors. The final column in this diagram displays the de-fuzzified GEFG values. Table 8 shows the GEFG values obtained for all twenty-seven experiments. Experiment Number 2 (spindle speed: 12,000 rpm, point angle: 118°, feed rate: 0.02 mm/rev, drill diameter: 6 mm) has the greatest GEFG value, showing the ideal combination of input elements for good drilling performance.

Table 8. Grey Relational Coefficients, Grey Relational Grade and Grey Entropy Fuzzy Grade (GEFG).

Experiment No.	Grey Relational Coefficients						GRG	GEFG
	Thrust Force (0.14)	Temperature (0.17)	Hole Size Error (0.17)	Circularity Error (0.13)	Peel-Up Delamination (0.23)	Push-Out Delamination (0.16)		
1	1.0000	0.7216	0.9275	1.0000	0.4004	0.7231	0.7794	0.750
2	0.9467	0.7143	0.7228	0.9012	0.6755	0.8131	0.8813	0.946
3	0.6992	0.6667	0.9801	0.9255	1.0000	0.9568	0.7790	0.650
4	0.7637	0.5109	0.9249	0.8752	0.7585	0.8736	0.8522	0.875
5	0.7225	0.6731	0.9638	0.9820	0.8372	0.9537	0.6335	0.625
6	0.6173	0.6863	0.8391	0.4237	0.6745	0.4845	0.7827	0.750
7	0.3333	0.8917	0.8398	0.8534	0.8234	0.8835	0.6265	0.625
8	0.5251	0.6306	1.0000	0.8953	0.4192	0.3936	0.7401	0.750
9	0.5822	0.6863	0.9573	0.9224	0.6348	0.7078	0.6875	0.725
10	0.7671	0.5224	0.6410	0.9224	0.5793	0.8076	0.8210	0.839
11	0.9265	0.7216	0.8306	0.7715	0.8234	0.8608	0.6642	0.675
12	0.8978	0.8917	0.7292	0.5156	0.4464	0.5831	0.7113	0.750
13	0.4245	0.3825	0.7123	0.8507	0.8483	1.0000	0.7255	0.750
14	0.7915	0.7368	0.9499	1.0037	0.4748	0.5516	0.7128	0.700
15	0.4795	1.0000	0.3333	0.9513	0.7991	0.6973	0.5891	0.500
16	0.8454	0.4516	0.8656	0.7207	0.3545	0.4476	0.7122	0.750
17	0.7225	0.5224	0.9629	0.9927	0.5375	0.6620	0.7868	0.750
18	0.6354	0.5303	0.9189	0.9513	0.8174	0.8736	0.7314	0.678
19	0.4592	0.3333	0.8341	0.9580	0.8861	0.8769	0.6600	0.628
20	0.9731	0.8974	0.7757	0.3333	0.5159	0.4835	0.6881	0.675
21	0.5802	0.6667	0.3364	0.9785	0.7991	0.7833	0.6576	0.675
22	0.9314	0.5645	0.9536	0.9892	0.3333	0.3990	0.6437	0.625
23	0.8100	0.4516	0.6104	0.4871	0.6911	0.7966	0.8008	0.750
24	0.6448	0.5983	0.9112	0.9927	0.8524	0.8048	0.6711	0.686
25	0.7347	0.5303	0.6550	0.9287	0.6027	0.6714	0.8177	0.788
26	0.9216	0.6195	0.7249	0.9319	0.8524	0.8935	0.6768	0.700
27	0.7671	0.8140	0.9724	0.9964	0.3602	0.3333	0.7794	0.750

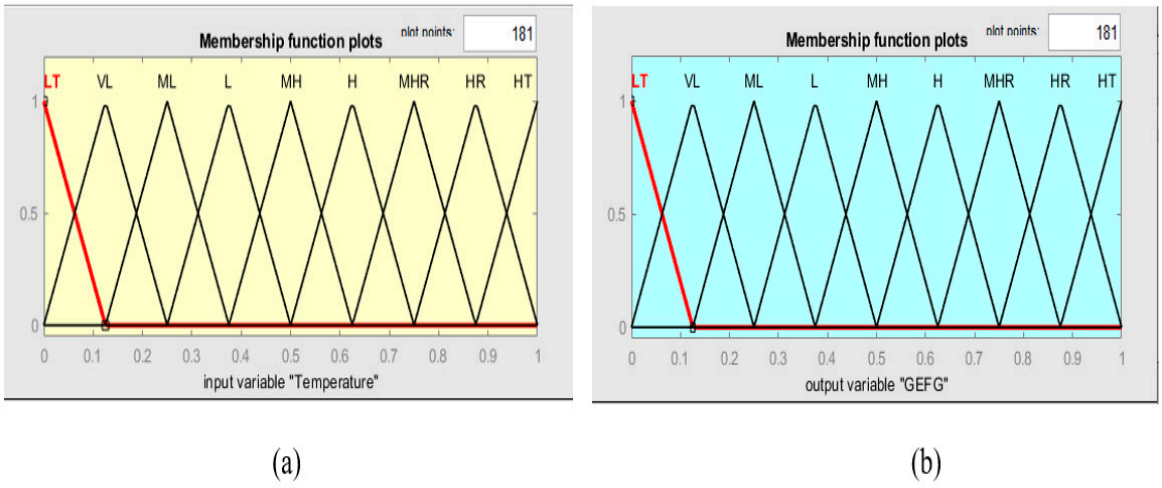

Figure 6. Membership functions for (**a**) input factors and (**b**) output GEFG.

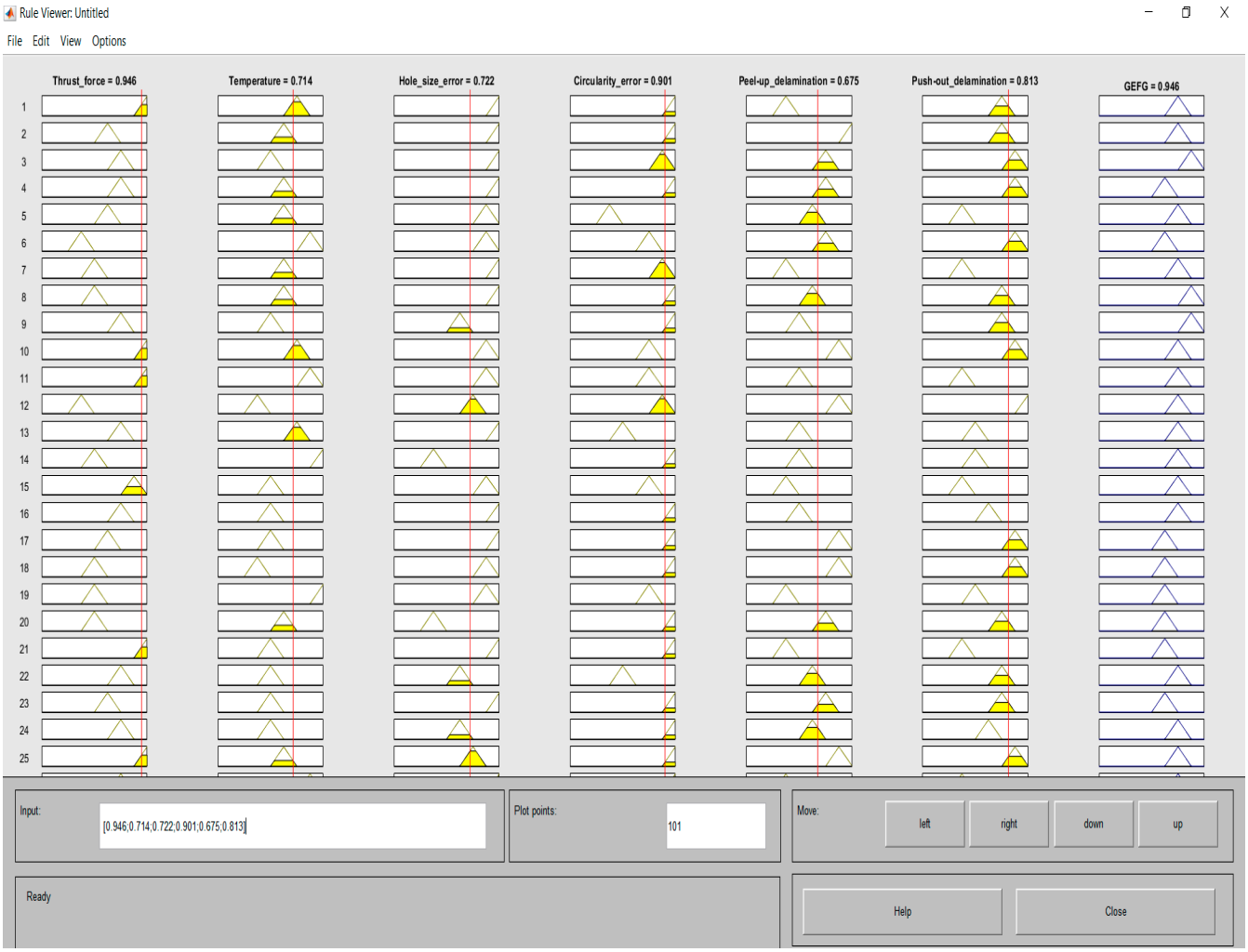

Figure 7. Fuzzy logic rule viewer of Experiment Number 2 (highest GEFG).

6. Conclusions

The input parameters considered in this study are spindle speed, feed rate, point angle and the diameter of the drill bit. The output factors (responses) are thrust force,

temperature, hole size error, circularity error, peel-up and push-out delamination factors and hole diameter. Based on the obtained results, the following conclusions are drawn:

- Temperature increases with increasing feed rates and spindle speeds. This is because increasing feed rates and spindle speeds increases the transformation of high energy and hence a higher dissipation of mechanical energy into heat.
- Thrust force was found to decrease with increasing speed rotation. This is thought to be due to matrix softening because of increased drilling temperatures.
- High spindle speeds with low feed result in a large hole size error due to the large frictional heating temperature at the tool–workpiece interface.
- Peel-up delamination at lower spindle speeds is much smaller than that at greater spindle speeds.
- Push-out delamination increases with an increase in both spindle speed and feed rate.
- Because of the above factor dependencies, the optimum requirements of output factors call for different combinations of input parameters.
- Considering all the responses simultaneously, using the Grey Entropy Fuzzy method, at a low level of spindle speed and feed rates (spindle speed: 12,000 rpm, and feed rate: 0.02 mm/rev) and moderate levels of the point angle and drill diameter (point angle: 118°, and drill diameter: 6 mm) the single optimum combination of machining conditions is indicated.

The conclusions are valid within the range of the process parameters chosen. Future research work may focus on a selection of additional levels of input parameters.

Supplementary Materials: The following supporting information can be downloaded at: https://www.mdpi.com/article/10.3390/pr10091865/s1, Table S1: Normalized, P_{ij}, and $P_{ij}\ln P_{ij}$ values for the responses.

Author Contributions: J.B.: data curation and writing—original draft preparation; A.M.: methodology; L.P.: formal analysis; A.N.K.A.: investigation, supervision; J.P.D.: project administration, supervision, validation. All authors have read and agreed to the published version of the manuscript.

Funding: This research received no external funding.

Data Availability Statement: Not applicable.

Acknowledgments: Authors Jalumedi Babu and A. N. Khaleel Ahmed acknowledge the support and encouragement given by Alice Abraham, President, and Paul Mathulla, Chairman, IMPACT Group of Institutions, Bangalore, India. All authors thank the editors and anonymous reviewers for their constructive comments and suggestions to improve the quality of this paper.

Conflicts of Interest: The authors declare no conflict of interest.

References

1. Shin, L.J.; Dassan, B.; Emayaruba, G.; Abidin, Z.; Shukur, M.; Anjang, A. Tensile and compressive properties of Glass Fiber-reinforced Polymer Hybrid Composite with Eggshell Powder. *Arab. J. Sci. Eng.* **2020**, *45*, 5783–5791. [CrossRef]
2. Reisgen, U.; Schiebahn, A.; Lotte, J.; Hopmann, C.; Schneider, D.; Neuhaus, J. Innovative joining technology for the production of hybrid components from FRP and metals. *J. Mater. Process. Technol.* **2020**, *282*, 116674. [CrossRef]
3. Bayraktar, S.; Turgut, Y. Determination of delamination in drilling of carbon fiber reinforced carbon matrix composites/Al 6013-T651 stacks. *Measurement* **2020**, *154*, 107493. [CrossRef]
4. Masoud, F.; Sapuan, S.M.; Mohd Ariffin, M.K.A.; Nukman, Y.; Bayraktar, E. Cutting processes of natural fiber-reinforced polymer composites. *Polymers* **2020**, *12*, 1332. [CrossRef]
5. Kopparthi, P.K.; Kundavarapu, V.R.; Kaki, V.R.; Pathakokila, B.R. Modeling and multi response optimization of mechanical properties for E-glass/polyester composite using Taguchi-grey relational analysis. *Proc. Inst. Mech. Eng. Part L J. Eng. Process.* **2021**, *235*, 342–350. [CrossRef]
6. Babu, J.; Sunny, T.; Paul, N.A.; Mohan, K.P.; Philip, J.; Davim, J.P. Assessment of delamination in composite materials: A review. *Proc. Inst. Mech. Eng. Part B J. Eng. Manuf.* **2016**, *230*, 1990–2003. [CrossRef]
7. Babu, J.; Philip, J.; Zacharia, T.; Davim, J.P. Delamination in composite materials: Measurement, assessment and prediction. In *Machinability of Fibre Reinforced Plastics*; De Gruyter: Berlin, Germany, 2015; pp. 139–162.
8. Sobri, A.S.; Whitehead, D.; Mohamed, M.; Mohamed, J.J.; Mohamad Amini, M.H.; Hermawan, A.; Norizan, M.N. Augmentation of the delamination factor in drilling of carbon fibre-reinforced polymer composites (CFRP). *Polymers* **2020**, *12*, 2461. [CrossRef]

9. Khashaba, U.A.; Abd-Elwahed, M.S.; Ahmed, K.I.; Najjar, I.; Melaibari, A.; Eltaher, M.A. Analysis of the machinability of GFRE composites in drilling processes. *Steel Compos. Struct.* **2020**, *36*, 417–426.
10. Khashaba, U.A.; El-Keran, A.A. Drilling analysis of thin woven glass-fiber reinforced epoxy composites. *J. Mater. Process. Technol.* **2017**, *249*, 415–425. [CrossRef]
11. Formisano, A.; Papa, I.; Lopresto, V.; Langella, A. Influence of the manufacturing technology on impact and flexural properties of GF/PP commingled twill fabric laminates. *J. Mater. Process. Technol.* **2019**, *274*, 116275. [CrossRef]
12. Erturk, A.T.; Vatansever, F.; Yarar, E.; Guven, E.A.; Sinmazcelik, T. Effects of cutting temperature and process optimization in drilling of GFRP composites. *J. Compos. Mater.* **2021**, *55*, 235–249. [CrossRef]
13. Ramesha, K.; Santhosh, N.; Kiran, K.; Manjunath, N.; Naresh, H. Effect of the Process Parameters on Machining of GFRP Composites for Different Conditions of Abrasive Water Suspension Jet Machining. *Arab. J. Sci. Eng.* **2021**, *44*, 7933–7943. [CrossRef]
14. Kao, W.H. Tribological prosperities and high-speed drilling application of MoS_2–Cr Coatings. *Wear* **2005**, *258*, 812–825. [CrossRef]
15. Lin, S.C.; Chen, I.K. Drilling carbon fiber reinforced material at high-speed drilling. *Wear* **1996**, *194*, 156–162. [CrossRef]
16. Rubio, C.J.; Abrao, A.M.; Faria, P.E.; Esteves Correia, A.; Davim, J.P. Effect of high speed in drilling of Glass Fiber Reinforced Plastic; Evaluation of delamination factor. *Int. J. Mach. Tools Manuf.* **2008**, *48*, 715–720. [CrossRef]
17. Rawat, S.; Atta, H. Charecterization of dry high-speed drilling process of woven composites using Machinability maps approach. *CIRP Ann. Manuf. Technol.* **2009**, *58*, 105–108. [CrossRef]
18. Krishnaraj, V.; Ramanathan, A.P.; Elanghovan, N.; Kumar, M.S.; Zitoune, R.; Davim, J.P. Optimization of machining parameters at high-speed drilling of carbon fiber reinforced plastic (CFRP) laminates. *Compos. Part B* **2012**, *43*, 1791–1799. [CrossRef]
19. Babu, J.; Paul, N.A.; Mohan, K.P.; Philip, J.; Davim, J.P. Examination and modification of equivalent delamination factor for assessment of high-speed drilling. *J. Mech. Sci. Technol.* **2016**, *30*, 5159–5165. [CrossRef]
20. Babu, J.; Paul, N.A.; Sonu, P.; Abraham, S.P.; Anoop, B.N.; Philip, J.; Davim, J.P. Development of comprehensive delamination factor and it's assessment of high-speed drilling. *Proc. Inst. Mech. Eng. Part B J. Eng. Manuf.* **2018**, *232*, 2109–2121. [CrossRef]
21. Abbas, C.A.; Huang, C.; Wang, J.; Wang, Z.; Liu, H.; Zhu, H. Machinability investigations on high-speed drilling of aluminium reinforced with silicon metal matrix composites. *Int. J. Adv. Manuf. Technol.* **2020**, *108*, 1601–1611. [CrossRef]
22. Zhang, L.; Wang, S.; Qiao, W.; Li, Z.; Wang, N.; Zhang, J.; Wang, T. High-speed milling of CFRP composites: A progressive damage model of cutting force. *Int. J. Adv. Manuf. Technol.* **2020**, *106*, 1005–1015. [CrossRef]
23. Jia, X.; Chen, Y.; Liu, L.; Wang, C.; Duan, J. Advances in Laser Drilling of Structural Ceramics. *Nanomaterials* **2022**, *12*, 230. [CrossRef]
24. Jia, X.; Chen, Y.; Liu, L.; Wang, C.; Duan, J. Combined pulse laser: Reliable tool for high-quality, high-efficiency material processing. *Opt. Laser Technol.* **2022**, *153*, 108209. [CrossRef]
25. Perec, A.; Musial, W. Multiple Criteria Optimization of Abrasive Water Jet Cutting Using Entropy-VIKOR Approach. In *Advances in Manufacturing Engineering and Materials II. ICMEM 2021.2Lecture Notes in Mechanical Engineering*; Hloch, S., Klichová, D., Pude, F., Krolczyk, G.M., Chattopadhyaya, S., Eds.; Springer: Cham, Switzerland, 2021; pp. 50–66.
26. Perec, A.; Musial, W.; Prazmo, J.; Sobczak, R.; Radomska-Zalas, A.; Fajdek-Bieda, A.; Nagnajewicz, S.; Pude, F. Multi-criteria Optimization of the Abrasive Waterjet Cutting Process for the High-Strength and Wear-Resistant Steel Hardox®500. In *Advances in Water Jetting. Water Jet 2019. Lecture Notes in Mechanical Engineering*; Klichová, D., Sitek, L., Hloch, S., Valentinčič, J., Eds.; Springer: Cham, Switzerland, 2021; pp. 145–154. [CrossRef]
27. Babu, J.; Madarapu, A.; Sunny, T.; Ramana, M.V. Multi characteristic optimization of high-speed machining of GFRP laminate by hybrid Taguchi desirability approach. *Mater. Today Proc.* **2022**, *58*, 238–243. [CrossRef]
28. Weinert, K.; Kempmann, C. Cutting temperatures and their effects on the machining behaviour in drilling reinforced plastic composites. *Adv. Eng. Mater.* **2004**, *6*, 684–689. [CrossRef]
29. Bogovič, V.; Svete, A.; Rupnik, K.; Bajsić, I. Experimental analysis of the temperature rise during the simulation of an implant drilling process using experimental designs. *Measurement* **2015**, *63*, 221–231. [CrossRef]
30. Feito, N.; López-Puente, J.; Santiuste, C.; Miguélez, M.H. Numerical prediction of delamination in CFRP drilling. *Compos. Struct.* **2014**, *108*, 677–683. [CrossRef]
31. Chatterjee, A. Thermal degradation analysis of thermoset resins. *J. Appl. Polym. Sci.* **2009**, *114*, 1417–1425. [CrossRef]
32. Yashiro, T.; Ogawa, T.; Sasahara, H. Temperature measurement of cutting tool and machined surface layer in milling of CFRP. *Int. J. Mach. Tools Manuf.* **2013**, *70*, 63–69. [CrossRef]
33. Khashaba, U.A. Drilling of polymer matrix composites: A review. *J. Compos. Mater.* **2012**, *47*, 1817–1832. [CrossRef]
34. Gaitonde, V.N.; Karnik, S.R.; Rubio, J.C.; Correia, A.E.; Abrao, A.M.; Davim, J.P. A study aimed at minimizing delamination during drilling of CFRP composites. *J. Compos. Mater.* **2011**, *45*, 2359–2368. [CrossRef]
35. Gaitonde, V.N.; Campos Rubio, J.; EstevesCorreia, A.; Abrão, A.M.; Paulo Davim, J. Delamination analysis in high speed drilling of carbon fiber reinforced plastics (CFRP) using artificial neural network model. *Mater. Des.* **2008**, *29*, 1768–1776.
36. Zou, Z.H.; Yun, Y.; Sun, J.N. Entropy method for determination of weight of evaluating indicators in fuzzy synthetic evaluation for water quality assessment. *J. Environ. Sci.* **2006**, *18*, 1020–1023. [CrossRef]
37. Sharma, P.; Singh, S.; Mishra, D.R. Electrical discharge machining of AISI 329 stainless steel using copper and brass rotary tubular electrode. *Procedia Mater. Sci.* **2014**, *5*, 1771–1780. [CrossRef]

38. Paul, L.; Babu, J.; Jose, S.; Babu, S. Application of grey fuzzy logic in abrasive jet machining process. *Sādhanā* **2022**, *47*, 1–9. [CrossRef]
39. Paul, L.; Hiremath, S.H.; Babu, J.; Libin, V.K. Effect of sensing mechanism on machining performance of ECDM process. *J. Adv. Mater. Process. Technol.* **2021**, *7*, 1–10. [CrossRef]
40. Vishnu, A.; Babu, J. Green supplier selection using hybrid grey relational analysis with fuzzy logic method. In *IOP Conference Series, Material Science and Engineering*; IOP Publishing: Bristol, UK, 2018; p. 012370.
41. Babu, J.; Anjaiah, M.; James, A. Optimisation and selection of forming depth and pressure of box shaped Superplastic forming using grey based fuzzy logic. In *IOP Conference series, Material Science and Engineering*; IOP Publishing: Bristol, UK, 2018; p. 012086.
42. Babu, J.; James, A.; Philip, J.; Chakraborty, S. Application of the grey-based fuzzy logic approach for materials selection. *Int. J. Mater. Res.* **2017**, *108*, 702–709. [CrossRef]
43. Kumar, J. Prediction of surface roughness in wire electric discharge machining (WEDM) process based on response surface methodology. *Int. J. Eng. Technol.* **2012**, *2*, 708–712.